Chapter 2
Single-Molecule Kinetic Analysis of Stochastic Signal Transduction Mediated by G-Protein Coupled Chemoattractant Receptors

Yukihiro Miyanaga and Masahiro Ueda

Abstract Cellular chemotactic behaviors are typical examples of stochastic signal transduction in living cells that have been investigated in detail both experimentally and theoretically. In this chapter, we describe single-molecule kinetic analysis for stochastic signal transduction in chemotactic responses mediated by G protein-coupled chemoattractant receptors in order to give deeper understanding of the stochastic nature in chemotactic signaling processes. We also describe theoretical analysis of receptor-mediated chemotactic signaling, which reveals that noise generated in the transmembrane signaling by G protein-coupled chemoattractant receptors limits the precision of the gradient sensing. This suggests that receptor-G protein coupling and its modulation have an important role for improving the signal-to-noise ratio of chemotactic signals and thus cellular chemotaxis. Extending this beyond G protein signaling, combining single-molecule kinetic analysis with theoretical analysis offers a new tool in exploring the relationship between the kinetic properties of signaling molecules and their corresponding cellular responses in general.

Keywords *Dictyostelium* · Chemoattractant · cAMP · GPCR · cAR1 · PTEN · PI3K · Crac · TIRFM · Halo · Chemotaxis · Noise · Fluctuation · *Gain-fluctuation relation* · GFR · SNR · Kinetic heterogeneity · Polarity

Y. Miyanaga (✉) and M. Ueda
Laboratories for Nanobiology, Graduate School of Frontier Biosciences, Osaka University, Suita, Osaka 565-0871, Japan
and
Japan Science and Technology Agency, Core Research for Evolutional Science and Technology, Suita, Osaka 565-0871, Japan
e-mail: yukihiro@phys1.med.osaka-u.ac.jp; ueda@phys1.med.osaka-u.ac.jp

Y. Sako and M. Ueda (eds.), *Cell Signaling Reactions: Single-Molecular Kinetic Analysis*, 33
DOI 10.1007/978-90-481-9864-1_2,

2.1 Introduction

Intracellular signal transduction has a stochastic nature due to its underlying chemical and physical reactions. For example, when an extracellular ligand binds stochastically to a cell's membrane receptors, the number of occupied receptors fluctuates with time and space in cells. The average of this number corresponds to concentrations of the extracellular ligand, while fluctuations in this number are considered a counting error, or noise, a result of the receptor's stochastic reactions. Downstream of the receptor are many types of signaling molecules involved in the signal processing and transduction. These molecules also operate stochastically, making the signal transmission inevitably noisy. Revealing how cells identify environmental cues enmeshed inside a noisy signal is crucial to further our understanding of the computational principles involved in intracellular signal transduction. This is an important question, as the stochastic computation systems in living cells are either noise-robust or noise-utilizing information processors that require far less energy than current artificial systems, and therefore offers a new design paradigm.

For such studies, single-molecule imaging has been successfully applied to a variety of biomolecules both in vitro and in living cells, leading to advances in the understanding of these molecules' stochastic nature [9, 42, 51, 54, 61]. Examples include the random transitions between open and closed states of single ion channels, stochastic behaviors in catalytic reactions done by single enzyme molecules, and stepwise motions of molecular motors [20, 23, 40]. In living cells, vital unitary reactions for signal transductions involving the signaling molecules like complex formations, conformational changes, and diffusion have been visualized at the single-molecule level [14, 41, 42, 54]. The stochastic properties of these reactions, such as the kinetic rates of the association and dissociation of complexes and diffusion coefficients, have been determined experimentally in the context of the cellular microenvironments. Intracellular microenvironments such as ion concentrations, lipid compositions, and cytoskeletal organizations have the potentials to provide variations for the properties of individual signaling molecules. In fact, various kinds of signaling molecules have been found to exhibit heterogeneity in their behaviors in relation to the spatiotemporal changes of the intracellular microenvironment [13, 27, 54]. Such information is lost when making ensemble measurements of a large number of molecules. Thus, single-molecule imaging analysis provides a unique tool for revealing the kinetic details of signaling molecules in living cells.

Similarly, theoretical approaches have been applied to reveal how stochasticity in molecular reactions affects cellular behaviors. For example, Berg and Purcell revealed that molecule counting noise generated by receptors limits the precision of chemoreception on measurements of chemical concentrations in bacteria chemotaxis [2]. Bialek and Setayeshgar compared theoretical and experimental studies on the chemotaxis of *Escherichia coli*, showing that the bacterial chemotaxis is performed near the physical limits in chemoreception [3]. For amoeboid chemotaxis, Tranquillo et al. described a stochastic model in which fluctuations in ligand-receptor binding reactions affect motile behaviors and limit chemotactic

accuracy [52]. However, these theoretical analyses have been performed despite knowing very little about the kinetic details of signaling molecules in living cells, and therefore further theoretical analyses are required to quantitatively describe the relationship between the inherent noise of the signaling molecules and the corresponding cellular response. Recently, Shibata and Fujimoto proposed the *gain-fluctuation relation* (GFR) for stochastic signal transduction, which can describe how stochastic noise is generated, amplified and propagated along a signaling cascade ([46], Chapter 13). Based on the kinetic properties of signaling molecules, the GFR can estimate the noise strength propagated along the signal transduction process.

In this chapter, we discuss the chemotactic signaling of eukaryote *Dictyostelium discoideum* cells as a typical example for stochastic signal transduction. Specific attention is given to single-molecule kinetic analysis and GFR-based theoretical analysis, which can quantitatively explain the stochastic cellular responses of this system by deriving the kinetic properties of the relevant signaling molecules.

2.2 Gradient Sensing and Directional Cell Migration in *Dictyostelium discoideum*

Dictyostelium discoideum is a well-established model organism for elucidating molecular mechanisms of amoeboid movements and regulation. This organism has many advantages for molecular and cellular biology studies including having its genome completely sequenced, well-established genetic engineering techniques, and advanced microscopic techniques [6, 11, 12, 32, 38, 62]. In addition, there are several more reasons why it is ideal for cellular motility research. For example, *Dictyostelium* cells are highly motile and exhibit fast amoeboid movements, with a velocity of 10–20 μm/min on glass substrates. The crawling movements on the surface take place spontaneously and randomly, even in the absence of extracellular cues [50]. Under a spatial heterogeneous environment of extracellular cues, cells exhibit tactic behaviors such as chemotaxis and electrotaxis [44, 48]. At the aggregation stage during their life cycle, cells exhibit chemotaxis in response to cyclic adenosine 3′5′-monophosphate (cAMP)(Fig. 2.1a), which induces multicellular organization [45]. About one hundred thousand of the cells move directionally toward the aggregation center by chemotaxis, and then form one multicellular aggregate. In this situation, more than 99% of cells exhibit synchronous chemotaxis, making it possible to prepare highly homogeneous cell populations. These properties have enabled investigators to study numerous essential intracellular activities including the roles of actin and microtubule cytoskeletons on cellular motility [11, 32, 62]. The molecular components required for chemotactic responses have been also identified extensively [12, 16, 33, 35, 43, 48]. Furthermore, imaging analysis of cytoskeletal proteins and their regulatory molecules has revealed the dynamic behaviors of these molecules during amoeboid movements in

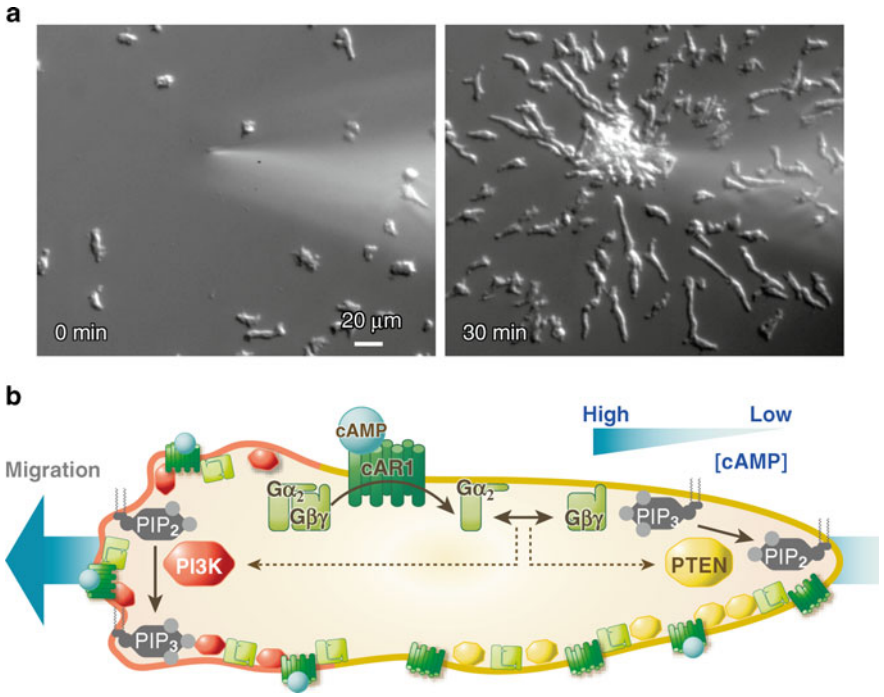

Fig. 2.1 Chemotactic signaling of *Dictyostelium* cells. (**a**) Chemotaxis of *Dictyostelium* cells toward the tip of a micropipette containing the chemoattractant cAMP. Images were captured at time 0 (*left panel*) and 30 min after (*right panel*) introduction of the micropipette. (**b**) cAMP signals are mediated by G protein-coupled cAMP receptors, especially cAR1. Receptor stimulation results in the activation and dissociation of heterotrimeric G protein, followed by the regulation of downstream signaling molecules such as PTEN and PI3K. PTEN catalyzes the dephosphorylation of PtdIns(3,4,5)P_3, while PI3K catalyzes the phosphorylation of PtdIns(4,5)P_2. Such antagonistic activities are essential for PtdIns(3,4,5)P_3 localization at the leading edge of chemotactic cells. Abbreviations: PTEN, phosphatase and tensin homologue deleted on chromosome 10; PI3K, phosphatidylinositol 3-kinase; PIP_2, phosphatidylinositol (4,5) bisphosphate or PtdIns(4,5)P_2; PIP_3, phosphatidylinositol (3,4,5) triphosphate or PtdIns(3,4,5)P_2.

response to chemotactic stimulations [5, 10, 12, 48]. In particular cases, signaling molecules have been observed at the single molecule level in living cells [27, 28, 31, 54, 57].

Chemotaxis is a fascinating phenomenon from the viewpoint of stochastic signal transduction in living cells. Cells show extreme sensitivity to subtle cAMP concentration gradients (Fig. 2.1b). The chemotactic ability of cells to cAMP gradients is studied quantitatively and signal inputs for chemotaxis are estimated [7, 26, 47, 55]. In a range of 0.1 nM to several μM cAMP, even a 2% gradient across the cell body can trigger a chemotactic response. When we consider a cell length of 10 μm with 80,000 receptors and $K_d = 100$ nM, for such a gradient (for example, ~3.3×10^{-3} nM/μm assuming 0.5 nM cAMP), the receptor occupancy is estimated to be ~400 molecules, while the difference in receptor occupancy between front and back halves of the cell is

only on the order of 10 molecules. Such a small difference suggests that the stochastic properties of the receptor may affect gradient sensing ability. Assuming a Poisson process, fluctuations in receptor occupancy equal the square root of the averaged occupancy, which for 400 occupied receptors translates to ~20 molecules, which is larger than the front-back differences. This means that stochastic fluctuations can reverse the ligand-binding patterns along the length of a cell even when the extracellular chemoattractant gradient is stationary, which implies that signal inputs for chemotaxis are noisy. Thus, *Dictyostelium* cells can sense a faint signal within stochastic noise. Understanding how the signaling system is designed to reliably obtain information in such an environment is an important issue in chemotaxis studies.

Signaling components and their reaction networks for chemotaxis are largely shared among many eukaryotic cells (Fig. 2.1b) [12, 16, 33, 35, 43, 48]. In *Dictyostelium* cells, chemotaxis in response to cAMP is mediated by G protein-coupled cAMP receptors (cARs). Among them, cAR1 functions dominantly at the aggregation stage. cAMP binding to cAR1 activates intracellular heterotrimeric G protein, which facilitates the G protein to separate into its two subunits, $G\alpha_2$ and $G\beta\gamma$. These subunits transduce signals that regulate downstream molecules including Ras, PI3K, PTEN, Crac, guanylyl cyclase, PLCγ, and PLA_2. One key reaction in this signaling system is the localization of phosphatidylinositol 3,4,5-trisphosphate (PtdIns(3, 4, 5)P_3) on the membrane side facing a higher concentration of cAMP. PtdIns(3, 4, 5)P_3 localization is regulated by PI3K and PTEN, which catalyze PtdIns(3, 4, 5)P_3 production and degradation, respectively. Because PI3K and PTEN are reciprocally localized on the membrane sides facing higher and lower cAMP concentration, respectively, PtdIns(3, 4, 5)P_3 accumulates at the leading edge of chemotaxing cells, acting as a cue for pseudopod formation to bias cell movement. Thus, a chemotactic signaling system can convert small differences in extracellular signals into localized signals that facilitate pseudopod formation and maintenance. PtdIns(3, 4, 5)P_3 localization takes place in an all-or-none manner with respect to the direction of the chemoattractant gradient [18], suggesting that noisy chemotaxis signals are somehow processed to consistently reflect the direction of the chemoattractant gradient. To understand how signal inputs for chemotaxis are received, processed and transduced by stochastically-operating signaling molecules, it is important to uncover the stochastic nature of the signaling molecules at work.

2.3 Single-Molecule Imaging Analysis of Chemotactic Signaling System in Living Cells

We have applied total internal reflection fluorescence microscopy (TIRFM) for single molecule imaging in a living cell (Fig. 2.2a). Originally, TIRFM was used for imaging multi-molecules and organelles in living cells [1], and has been further refined for single-molecule imaging of biomolecules [9, 42, 51, 54]. The theoretical aspects of TIRFM are discussed elsewhere [1, 8, 59]. Also, experimental apparatus and sample preparation for *Dictyostelium* cells are described previously in detail [28, 31].

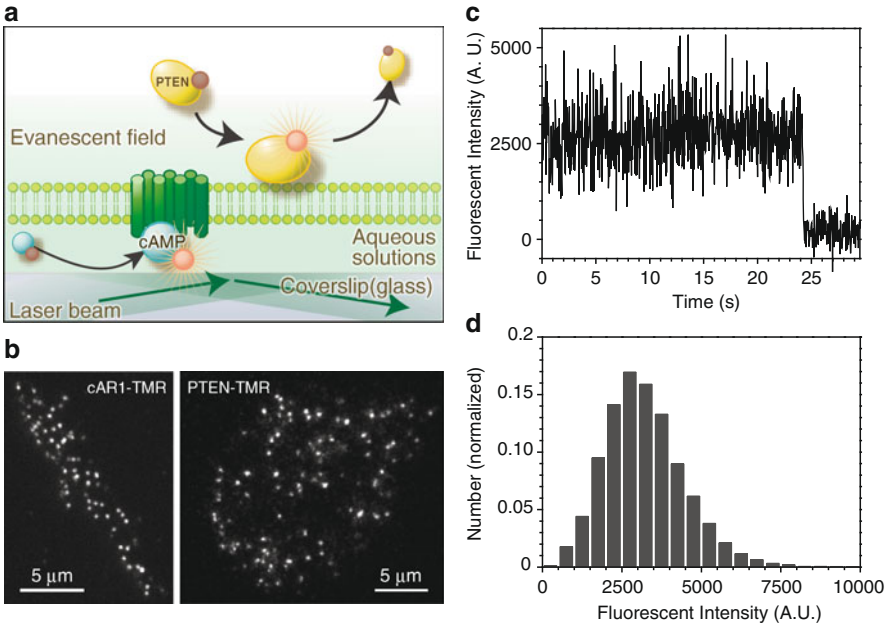

Fig. 2.2 Single molecule imaging in living cells. (**a**) Schematic drawing of single molecule imaging. The basal membrane of a *Dictyostelium* cell is illuminated by evanescent fields generated by the total internal reflection of an incident laser. Diffusible fluorescent molecules in the cytoplasm or extracellular aqueous solution, such as PTEN-TMR and Cy3-cAMP, are not seen due to their rapid diffusions. However, their fluorescence can be seen when these molecules bind to the plasma membrane or membrane-bound receptors. (**b**) Typical images of single-molecules of cAR1-TMR (*left panel*) and PTEN-TMR (*right panel*). (**c**) Typical time course of the fluorescence intensity arising from a single cAR1-TMR spot showing single-step photobleaching. (**d**) Distribution of cAR1-TMR fluorescence intensities.

Target molecules for single-molecule imaging by TIRFM should be labeled with a fluorescent dye, which must be selected with care. In order to conduct kinetic analysis through single-molecule imaging, we need fluorophores that do not interfere with the function of the molecule. Also, fluorescent dyes that have a bright fluorescent intensity and are stable over a long observation time are preferred. Commonly used labels include green fluorescent protein (GFP or its variants) or a tag protein such as HaloTag [17, 27, 28]. We have applied several fluorescent-labeling techniques to *Dictyostelium* cells, having examined the photobleaching time of the label and signal-noise ratio of the acquired images. Currently, we find that HaloTag labeling is best for the single molecule imaging of signaling molecules in *Dictyostelium* cells.

In the HaloTag labeling method, the gene encoding target protein is fused to the HaloTag gene and transferred into the cells. There, the HaloTag-conjugated proteins are labeled specifically by treating with a fluorescent HaloTag ligand like tetramethylrhodamine (TMR). Using our equipment, TMR has both better brightness and

a longer photobleaching time than fluorescent proteins such as GFP or YFP. In fact, we can observe individual single molecules in living cells for tens of seconds or more under continuous excitation. Moreover, the labeling efficiency can be controlled to a level suitable for single-molecule imaging by adjusting the amount of HaloTag ligand. Labeling efficiency is sometimes problematic for single-molecule analysis because a high density of labeled molecules makes it difficult to identify single molecules. Therefore, the labeling efficiency should be such that overlapping between fluorescent spots when the molecules exhibit rapid diffusion is avoided. Empirically, the densities of the fluorescent spots should be limited to less than ~0.1 molecule/μm^2 for molecules with diffusion coefficients of ~0.2 $\mu m^2/s$ and less than ~0.7 molecule/μm^2 for molecules with diffusion coefficients of ~0.02 $\mu m^2/s$.

The simplest way to verify the functionality of the labeled molecules is to substitute these with native molecules, which can be easily done in *Dictyostelium* cells [15, 21, 25]. Using this haploid organism, functional fusion proteins for chemotactic signaling molecules including cAMP receptor, subunits of trimeric G protein, PI3K and PTEN have been successfully generated. Halo-tagged cAR1, $G\alpha_2$, $G\gamma$ and PTEN molecules can be confirmed as functional by examining whether the Halo-tagged genes for these molecules can rescue phenotypic defects in cells lacking the corresponding genes [28]. For instance, PTEN knockout cells exhibit severe defects in cell division, morphology and chemotactic movement. When HaloTag-conjugated PTEN (PTEN-Halo) is introduced, the transformed *pten*-null cells behave like wild type cells. PTEN-Halo was visualized by staining with TMR (PTEN-TMR), revealing a uniform localization on the membrane, as expected for functional PTEN molecules. When a fluorescent analogue of an extracellular ligand like chemoattractant is used for single molecule imaging analysis, it is also important to confirm whether the labeled analogue can activate the corresponding signaling pathways. We have generated a fluorescent analogue for cAMP (Cy3-cAMP) to monitor the signal inputs for chemotaxis [18, 54]. Cy3B-cAMP, which is commercially available (Amersham LKB, a component of cAMP Fluorescence Polarization Immunoassay kit, RPN3595), can also be used.

Figure 2.2b shows a typical example of fluorescent spots arising from TMR-labeled cAR1-Halo (cAR1-TMR) on the basal membrane of living *Dictyostelium* cells. To verify that the fluorescent spots represent single cAR1-TMR molecules, some characteristic features of a single molecule should be confirmed. One is single-step photobleaching, which occurred upon continuous excitation (Fig. 2.2c), and is consistent with the photobleaching of single fluorescent molecules. The histogram for cAR1-TMR fluorescence intensity exhibited a Gaussian distribution with a single mean value (Fig. 2.2d), which is also characteristic of single fluorescent molecules. For a mixture containing dimer and monomer molecules, the distribution of the fluorescence intensities should exhibit a sum of two Gaussian distributions.

Using the same experimental setup, PTEN-TMR on the basal membrane of living *Dictyostelium* cells can also be observed (Fig. 2.2b). PTEN molecules undergo dynamic shuttling between the membrane and cytoplasm. PTEN-TMR fluorescent spots behave differently from those of cAR1-TMR. Free PTEN-TMR molecules in

the cytosol cannot be imaged clearly as fluorescent spots at video frame rates because of rapid Brownian motion. When PTEN-TMR binds to membrane, however, diffusible movements slow due to its association, which allows for the visualization of clearly resolved TMR fluorescence spots (Fig. 2.2b). Following PTEN-TMR release from the membrane, the fluorescent spot suddenly disappears. Thus, association/dissociation events of a single signaling molecule on the membrane can be visualized in living cells. Additionally, the lateral diffusion of PTEN-TMR molecules can be observed simultaneously with association/dissociation reactions. Signaling molecules shuttling between the membrane and cytoplasm should also have a fluorescence intensity that exhibits a single-step disappearance and a quantized distribution. However, the disappearance of fluorescent spots should not necessarily be regarded as photobleaching because molecules may dissociate from the membrane before photobleaching occurs.

By analyzing the behaviors of individual molecules on the membrane statistically, their kinetic information such as dissociation rates of signaling complex can be obtained. Statistical analysis of the lateral diffusion is described in detail in Chapter 12 [29]. Here we explain briefly single-molecule kinetic analysis of signaling molecules for a simple case [28, 31]. First, the time duration between the appearance and disappearance of individual molecules on cells is measured. Then, the distribution of the time duration is constructed by counting the fraction of the duration. The number at $t = 0$ is the total number of molecules measured, which decays with time because of dissociation. Figure 2.3 shows a normalized distribution, also known as a cumulative probability distribution. Cumulative probability distributions of the time duration can be fitted with the following equation,

$$f(t) = a_1 \exp(-k_1 t) + a_2 \exp(-k_2 t) + \cdots \tag{2.1}$$

where k_i represents the dissociation rates and a_i represents the relative amount of the ith component. Summing a_i over all i equals 1. Inversing k_i gives the lifetimes, τ_i, of the molecules.

When membrane-integral proteins such as receptors are observed and analyzed, the distribution of the time duration reflects the photobleaching events because membrane-integral proteins do not dissociate from the membranes. Figure 2.3a show the cumulative probability distributions of cAR1-TMR and cAR1-YFP. The distribution of cAR1-TMR is well fitted to a single exponential curve with the time constant $\tau = 11$ s ($k_{bleaching} = 0.09\ \mathrm{s}^{-1}$), which represents the photobleaching time constant of TMR in living cells under our experimental system. On the other hand, cAR1-YFP has two time constants, $\tau_1 = 0.52$ s (86%) and $\tau_2 = 2.2$ s (14%). The multiple time constants suggests that YFP frequently exhibits photoblinking [30] (Fig. 2.3b). The shorter observable time and complicated photo-stability of YFP may cause misinterpretations of data for YFP-tagged target proteins.

For molecules dynamically shuttling between the membrane and cytosol, the cumulative probability distribution of the molecules reflects the release from the membrane if the dissociation rates of the molecules are relatively faster than

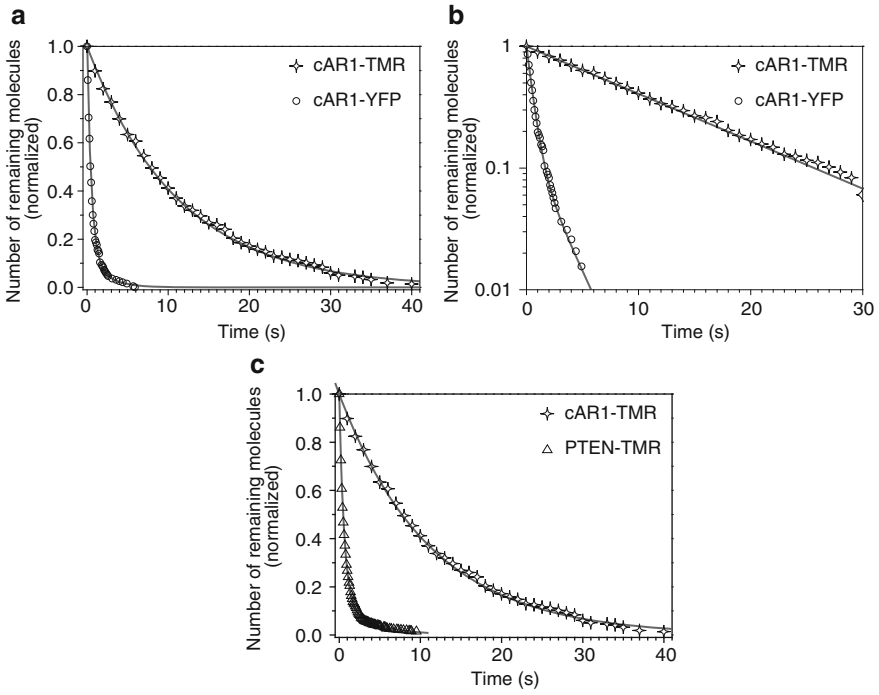

Fig. 2.3 Lifetime analysis of cAR1 and PTEN. (**a**) Cumulative probability distributions of cAR1-TMR (*stars*) and cAR1-YFP (*circles*). *Solid lines* represent the fitting curves of the data to a single exponential function with a time constant of 11 s (cAR1-TMR) and sum of two exponential functions with time constants of 0.52 s (86%) and 2.2 s (14%) (cAR1-YFP). (**b**) Semi-logarithmic plots of cumulative probability distributions facilitate the distinction between multiple and single time constant in the reaction. (**c**) Comparison of the lifetimes of cAR1-TMR (*stars*) and PTEN-TMR (*triangles*). Shorter lifetime of PTEN-TMR indicates the dissociation of PTEN-TMR from the membrane prior to the photobleaching of TMR.

the photobleaching rates of the fluorescence dyes. For example, the lifetimes of PTEN-TMR (0.6 s, 87% and 4.1 s, 13%) without correction are significantly shorter than that of cAR1-TMR (Fig. 2.3c), meaning that PTEN molecules dissociate from the membrane before photobleaching. Because the dissociation rates k_i obtained from Eq. 2.1 for experimental data are apparent values, they should be corrected by incorporating the photobleaching rate $k_{bleaching}$. The actual dissociation rates are obtained by subtracting the photobleaching rate from the apparent dissociation rates: $k = k_1 - k_{bleaching}$. The lifetime analysis of membrane-integral proteins such as receptors is sometimes performed as a control for signaling molecules that exhibit dynamic shuttling between the membrane and cytosol. Lifetime analysis has been successfully applied to kinetic studies of ligand-receptor complexes and downstream molecules including G-protein, PTEN and PH domain-containing proteins, as described below [27, 28, 54, 57].

2.4 Single-Molecule Kinetic Analysis of Stochastic Signal Inputs for Chemotaxis

To elucidate how *Dictyostelium* cells sense the chemoattractant cAMP, fluorescently-labeled cAMP (Cy3-cAMP) was prepared and its binding to the receptors on the cells was observed by using TIRFM (Fig. 2.4a) [54]. When Cy3-cAMP solution

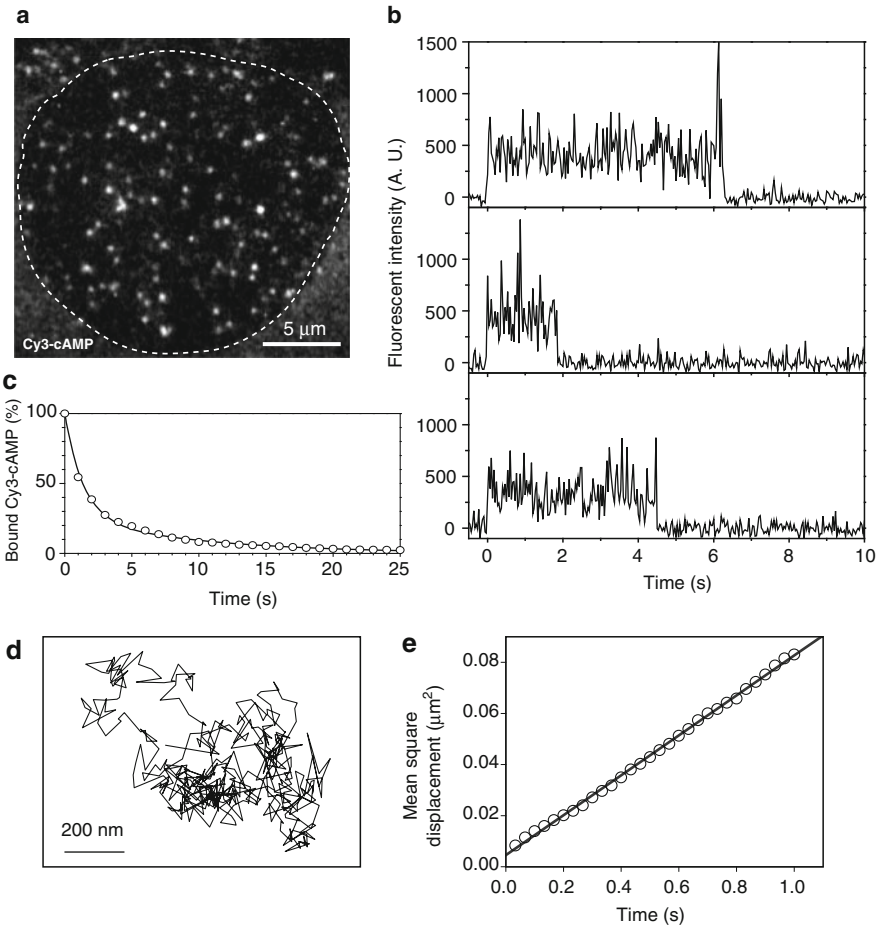

Fig. 2.4 Single molecule imaging analysis of signal inputs for chemotactic responses. (**a**) Typical image of Cy3-cAMP single-molecules. Cell contour is shown by *broken line*. (**b**) Typical time courses of fluorescence intensity from single Cy3-cAMP spots showing association and dissociation events between Cy3-cAMP and cAR1. Cy3-cAMP molecules bound to the receptor at time 0. (**c**) Cumulative probability distribution of Cy3-cAMP. (**d**) Typical single-molecule trajectory of Cy3-cAMP bound to its receptor on a living cell. Time length of the trajectory, 15.4 s. (**e**) Plot of the mean-squared displacement versus time, indicating that the receptor diffuses by simple Brownian motion with a diffusion coefficient of ~ 0.02 $\mu m^2/s$.

was applied to the cells, the fluorescence arising from the Cy3-cAMP molecule became visible as a single spot on the membrane, followed by the spot undergoing lateral diffusion and then suddenly disappearing (Fig. 2.4b). The cumulative probability distribution of Cy3-cAMP lifetimes were well fitted to a sum of exponential curves with constants of 0.93 s^{-1} (61%) and 0.11 s^{-1} (39%), which correspond to lifetimes of 1.1 and 8.2 s, respectively (Fig. 2.4c). These constants represent the dissociation rates of Cy3-cAMP-receptor complexes. In a simple kinetic scheme, ligand-binding reactions can be written as $R + L \leftrightarrow RL$, where R and L represent a receptor and ligand, respectively. The dissociation rates represent the rates for the state transition RL to R. Multiple dissociation rates indicate the receptor takes multiple kinetic states. Exponential distributions of the ligand-binding lifetimes demonstrate that the ligand dissociates from the receptor randomly. The majority of Cy3-cAMP-receptor complexes adopted the faster-dissociation state, meaning that the cells sense the chemoattractant within a 1 s sampling time. Lateral diffusion also can be analyzed simultaneously for individual Cy3-cAMP-bound receptors by calculating the mean square displacement (Fig. 2.4d, e) [29]. The diffusion coefficient of the individual Cy3-cAMP-receptor complex was ~0.02 $\mu m^2/s$. cAR1-Halo expressed in wild-type cells had a diffusion coefficient of ~0.02 $\mu m^2/s$ irrespective of cAMP being present, suggesting that ligand-binding to the cAR1 receptor does not affect lateral mobility on the membrane.

Single-molecule imaging of cAMP binding to the receptor in living cells can be also used to examine the receptor occupancy for chemotaxis. By counting the number of Cy3-cAMP complexes bound to a chemotaxing cell, the cell's receptor occupancy was determined, although the region measured was restricted to the cell's basal surface. Figure 2.5a shows an example of the temporal changes in

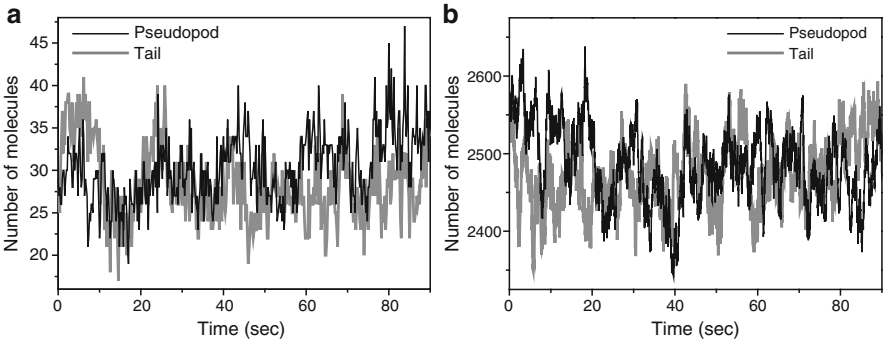

Fig. 2.5 Fluctuations in chemotactic signaling inputs. (**a**) Temporal changes in the number of bound cAMP molecules were measured by counting Cy3-cAMP spots on the anterior pseudopod (*black line*) and the posterior tail (*gray line*). (**b**) Numerical simulations of signal inputs. Temporal changes in the receptor occupancy in the anterior (*black line*) and posterior (*gray line*) halves of a single cell were simulated. It is assumed that the receptor adopt two states: fast- (dissociation rate, 1.0 s^{-1}; association rate, 4×10^{-6} $M^{-1}s^{-1}$; 78,000 molecules/cell) and slow-dissociating (dissociation rate, 0.04 s^{-1}; association rate, 4×10^{-6} $M^{-1}s^{-1}$; 4,000 molecules/cell).

receptor occupancy of a chemotaxing cell. The time series of the receptor occupancy at the anterior and posterior halves of the cell occasionally reverse against the direction of the cAMP gradient due to stochastic fluctuations in the ligand-receptor binding reaction. In other words, the posterior end may have higher occupancy despite the gradient being higher at the anterior. Thus, signal inputs on the basal surface of a chemotaxing cell are quite noisy. But we should note that the time series of the receptor occupancy does not represent the total inputs made by the chemotactic signals. This means we cannot exclude the possibility that such reversals are rare events when considering the cell's entire surface. Next, we performed a numerical simulation of ligand binding to the receptors (Fig. 2.5b). For simplicity, we assume that the receptors adopt slower- or faster-dissociating states stably without state transitions and that they are uniformly localized on the membrane. Also, we assume a Poisson process for the ligand-binding reaction. When the cAMP gradient across the cell body is 2% at 10 nM, differences in receptor occupancy between anterior and posterior halves of a cell can sometimes be negative, meaning that the ligand-binding patterns on the cell are reversed against the ligand concentration gradients. For direct measurements of total receptor occupancy over the whole surface of chemotaxing cells, further technical developments are required including numerical simulations [36, 37].

2.5 Stochastic Signal Transduction and Processing by Chemoattractant Receptors

As described in Section 2.4, chemoattractant receptors have been revealed to operate stochastically in living cells. Here we discuss the application of the *gain-fluctuation relation* (GFR) to transmembrane signaling initiated by chemoattractant receptors [46, 53]. A detailed explanation of the GFR is described in Chapter 13. The GFR can describe noise generation, amplification and propagation along a signaling cascade based on the kinetic properties of signaling molecules.

Let us consider a simple model for transmembrane signaling in which ligands bind to receptors stochastically to activate the receptors and initiate second messengers that act as stochastic signal outputs (Fig. 2.6a). The scheme is as follows:

$$\mathrm{R} + \mathrm{L} \underset{k_{off}}{\overset{k_{on}}{\leftrightarrow}} \mathrm{R}^*, \quad \mathrm{R}^* + \mathrm{X} \overset{k_p}{\rightarrow} \mathrm{R}^* + \mathrm{X}^*, \quad \mathrm{X}^* \overset{k_d}{\rightarrow} \mathrm{X}, \tag{2.2}$$

where R, R* and L represent inactive receptors, active receptors and ligands, respectively. X and X* are inactive and active forms of second messengers. k_{on} and k_{off} represent ligand-association and dissociation rates, respectively. k_p and k_d represent production and degradation rates for the second messenger, respectively. The average number of active receptor R^* and second messenger X^* per one cell can be given by,

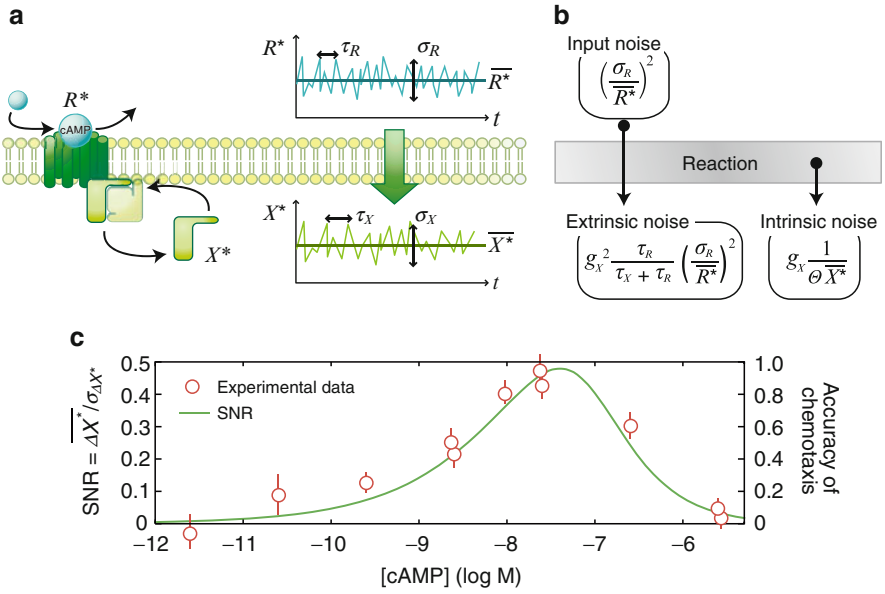

Fig. 2.6 Noise propagation and generation in chemotactic responses. (**a**) Simple model for transmembrane signaling. Ligand bound receptor becomes active (R*) and then activates second messenger (X*). Both input and output signal should have noise (σ_R and σ_X, respectively) around their averages ($\overline{R^*}$ and $\overline{X^*}$, respectively). (**b**) Noise generation and propagation. Input noise is propagated through the reaction as an extrinsic noise. Moreover, the reaction itself generates intrinsic noise. (**c**) Comparison of the theoretically obtained SNR (*line*) with experimental data (*circles*) for chemotactic accuracy of Dictyostelium cells.

$$\overline{R^*} = R_{total} \cdot L \cdot (K_R + L)^{-1}, \quad \overline{X^*} = X_{total} \cdot \overline{R^*} \cdot \left(K_X + \overline{R^*}\right)^{-1}, \tag{2.3}$$

where R_{total} is the total molecular number of receptors per single cell, $K_R = k_{off}/k_{on}$ is the affinity for the ligand-receptor binding reaction, X_{total} is the total molecular number of second messengers per cell, $K_X = k_d/k_p$ is the molecular number of active receptors when the activation of the second messenger reaches its half-maximum. Eq. 2.3 represents the input-output relationship between the average number of active receptor $\overline{R^*}$ and the average number of active second messenger $\overline{X^*}$ at ligand concentration L. According to the GFR [46], the relationship between the noise of the active receptor $(\sigma_X{}^2)$ and the noise of the active second messenger $(\sigma_X{}^2)$ is given by,

$$\frac{\sigma_X{}^2}{\overline{X^*}^2} = g_X \frac{1}{\Theta \overline{X^*}} + g_X{}^2 \frac{\tau_R}{\tau_X + \tau_R} \frac{\sigma_R{}^2}{\overline{R^*}^2}, \tag{2.4}$$

where Θ is a factor to adjust the dimension. $\Theta = 1$ when X^* is measured as a molecular number [46]. τ_R and τ_X are the chara?cteristic time constants of the

fluctuations in the ligand-binding and G protein activation reaction, respectively. According to scheme (2.2), the time constants are given by,

$$\tau_R = (k_{on}L + k_{off})^{-1}, \qquad \tau_X = \left(k_p\overline{R^*} + k_d\right)^{-1} \tag{2.5}$$

The gain, g_X, quantifies the amplification rate of the output responses to small changes in input, and is given by,

$$g_X = \frac{\Delta X/\overline{X}}{\Delta R^*/\overline{R^*}} = \frac{d\log X}{d\log R^*} = K_X \cdot \left(K_X + \overline{R^*}\right)^{-1} \tag{2.6}$$

Equation 2.4 describes the input-output relationship between noise in the active receptor concentration and noise in the active second messenger concentration (Fig. 2.6b). The second term on the right hand side of Eq. 2.4 represents the noise propagated from ligand-receptor binding reactions, which is modulated by the time constants τ_R and τ_X and the gain g_X. These parameters can be obtained from the rate constants k_{on}, k_{off}, k_p, and k_d of the signal transduction reaction. In some cases (e.g., k_{off}), the rate constants can be obtained directly by single-molecule experiments. The first term on the right hand side of Eq. 2.4 represents noise generated intrinsically by the second messenger production reaction itself. So even if noise propagated from the ligand-receptor binding reactions is negligible, intrinsic noise is still present. Thus, Eq. 2.4 describes how the kinetic properties of signaling molecules determine both signal and noise transmitted in the corresponding signaling reaction.

We next discuss chemotactic signaling based on the GFR. It is evident that eukaryotic amoeboid cells detect differences in chemoattractant concentrations across their cell body by the fact that they can extend pseudopods toward the chemical gradient without any cellular translocations [4, 34, 63]. This type of gradient sensing is known as spatial-sensing. Chemotactic signals in using a spatial-sensing mechanism originate from differences in the receptor occupancy between the anterior and posterior halves of a cell under a chemical gradient. Recently, the local excitation global inhibition (LEGI) mechanism was proposed as an extended spatial-sensing mechanism. The LEGI mechanism argues that spatial differences in the ligand concentration are sensed by comparing the excitatory signals derived from the receptor occupancy in a local area with the inhibitory signals derived from the average level of receptor occupancy over the entire surface of the cell [16, 24]. This mechanism does not entail direct comparison of the ligand concentration between different points over the cell surface. Instead, differences in receptor occupancy between a local area and the entire surface of the cell determine the chemotactic signal.

Here we consider the spatial-sensing mechanism for simplicity. We assume no polarity in the transmembrane signaling process along the length of a chemotaxis cell. In other words, the kinetic properties of the signaling molecules in the anterior and posterior halves of the cell are the same. A concentration difference in ligands

produces a difference in the receptor occupancy, ΔR^*, which then leads to a difference in active second messengers, ΔX^*, between the anterior and posterior region of the chemotactic cells. ΔR^* and ΔX^* should fluctuate with time and include noise $\sigma_{\Delta R}$ and $\sigma_{\Delta X}$, respectively. From the GFR, we obtain the following relation between $\sigma_{\Delta k}/\overline{\Delta R^*}$ and $\sigma_{\Delta x}/\overline{\Delta X^*}$,

$$\left(\frac{\sigma_{\Delta X}}{\overline{\Delta X}}\right)^2 = \frac{1}{g_X \Theta \overline{X^*}} \left(\frac{\overline{R^*}}{\overline{\Delta R^*}}\right)^2 + \frac{\tau_R}{\tau_X + \tau_R} \left(\frac{\sigma_{\Delta R}}{\overline{\Delta R^*}}\right)^2, \tag{2.7}$$

where the first term on the right hand side of Eq. 2.7 is derived from the noise generated intrinsically in the second messenger production reaction, while the second term is derived from the noise propagated from the ligand-receptor binding reaction [53].

We defined the SNR of the chemotactic signals as $\overline{\Delta X^*}/\sigma_{\Delta X}$, which is obtained from Eq. 2.7,

$$SNR = \frac{\overline{\Delta X^*}}{\sigma_{\Delta X}} = \frac{1}{\sqrt{4\left(\frac{L+K_R}{K_R}\right)\left\{\frac{(L+K_{XR})^2}{V_X \cdot K_{XR}} + \frac{\tau_R}{\tau_X+\tau_R}\left(\frac{L+K_R}{R_{total}}\right)\right\}}} \left(\frac{\Delta L}{\sqrt{L}}\right), \tag{2.8}$$

where $K_{XR} = K_X \cdot K_R \cdot (R_{total} + K_X)^{-1}$ is the ligand concentration when X^* is at half maximum and $V_X = R_{total} \cdot X_{total} \cdot (R_{total} + K_X)^{-1}$. By using parameter values obtained experimentally for *Dictyostelium* cells, we obtained the dependence of the SNR on cAMP concentration with a constant 2% gradient (Fig. 2.6c) ([53] for details of parameter values). We found a good agreement between our theoretical SNR and experimental data on the chemotactic accuracy of *Dictyostelium* cells [7, 53]. This suggests that chemotactic accuracy is determined mostly by the SNR of chemotactic signals at the most upstream reactions of the chemotactic signaling system. The SNR is proportional to $\Delta L/\sqrt{L}$ when ligand concentration is much smaller than $K_R$and K_{XR}. Supposing that cells can sense the gradient if the SNR of chemotactic signals is larger than the threshold SNR, or $SNR_{threshold} \leqslant C(\Delta L/\sqrt{L})$ with constant C, we find $\Delta L \geqslant \sqrt{L}\,(SNR_{threshold}/C)$for chemotaxis. Therefore, the minimum difference in ligand concentration necessary for chemotaxis is proportional to the square root of L, $\Delta L_{threshold} \propto \sqrt{L}$. In fact, Van Haastert and a colleague [56] reported the relation between the average concentration of ligand and the corresponding threshold gradient, estimating α in the relation $\Delta L_{threshold} \propto L^{\alpha}$ to be 0.5. We should note that Eqs. 2.7 and 2.8 are applicable to other cell types. In fact, similar dependency for chemotactic accuracy has been observed in mammalian leukocytes and neurons [39, 64].

Equations 2.7 and 2.8 can reveal the regulatory mechanisms used for signal improvements [53]. The SNR of the chemotactic signals is determined by the kinetic parameters of both the receptor and the downstream second messenger (k_{on}, k_{off}, k_p, k_d, K_X and K_R) along with their respective quantities (R_{total} and X_{total}). Therefore, changing a number of parameters individually potentially reveals a great

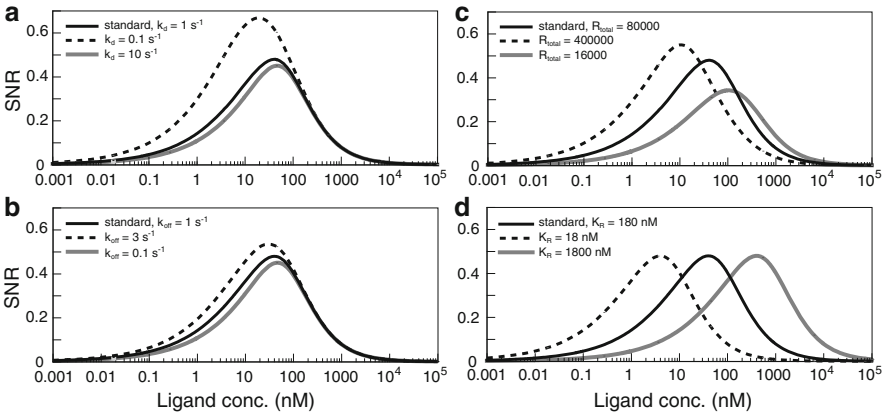

Fig. 2.7 Signal improvements. (**a**) Time-averaging effects. The SNR was improved by increasing the time constants of the second messenger. The degradation rates (k_d) were changed and the corresponding SNR was calculated: (*gray line*) 10 s^{-1}; (*black line*) 1 s^{-1}; (*broken line*) 0.1 s^{-1}. (**b**) Receptor fluctuation-dependent signal improvements. The dissociation rates of the ligand (k_{off}) were: (*gray line*) 0.1 s^{-1}; (*black line*) 1 s^{-1}; (*broken line*) 3 s^{-1}. (**c**) Dependency of the SNR on receptor expression levels. The receptor numbers are 16,000 (*gray*), 80,000 (*black*), 400,000 (*broken*) molecules/cell. (**d**) Effects of affinity modulation on the SNR. Ligand-binding affinity: 18 nM (*broken*), 180 nM (*black*), and 1,800 nM (*gray*).

deal about the relationship between the kinetic properties of signaling molecules and the corresponding cellular response.

The first example is how the SNR can be improved by increasing τ_X (Fig. 2.7a). The second term on the right hand side of Eq. 2.7 describes how the noise of the active receptor, R^*, propagates into the noise of the second messenger X^*. The term $\tau_R/(\tau_X + \tau_R)$ is known as the time-averaging factor of the noise. When the time constants of the second messenger production are faster than those of the active receptor $(\tau_X \ll \tau_R)$, the noise of the active receptor propagates more efficiently into the noise of the second messenger because the term $\tau_R/(\tau_X + \tau_R)$ increases gradually with a decrease in τ_X. In this case, the second messenger reaction can follow rapid temporal changes of the active receptor. On the other hand, in the case of $\tau_X \gg \tau_R$, the second messenger reaction cannot follow the noise of the active receptor. Instead, the noise of the active receptor is averaged temporally. Thus, in order to reduce the noise generated at the ligand-binding reaction, a relatively slower reaction is required during second messenger production. A longer second messenger lifetime, which corresponds to slower degradation, causes noise reduction more effectively by time-averaging effects (Fig. 2.7a). This means that the regulatory mechanism for degradation or inactivation of second messengers has a pivotal role on signal improvements for chemotaxis. In the case of G-protein, lifetimes of its active form on the membrane affect the SNR of the chemotactic signal, which is determined by both GTPase activity and its membrane-binding stability. In our

preliminary single-molecule analysis of $G\alpha_2$ and $G\beta\gamma$, receptor stimulation causes an enhancement in the membrane-binding stability of both subunits, suggesting that the SNR of the chemotactic signal is improved by modulating the lifetimes of G-protein on the membrane.

Second, the SNR can be improved by decreasing τ_R (Fig. 2.7b). When ligand concentration is increased, the ligand-binding rate, $k_{on}L$, accelerates, resulting in a decrease in the time constant τ_R (Eq. 2.5). Moreover, signal improvements are possible by increasing the on-rate (k_{on}) and/or off-rate (k_{off}). This means that faster transitions between the ligand-binding and -unbinding states of the receptors can produce chemotactic signals with higher SNR. That is, an increase in ligand concentration results in better efficiency of chemotactic signals not only by increasing the average concentration of the active receptor but also by decreasing the characteristic time of the active receptor fluctuations. As described below in Section 2.6, chemotactic cells that exhibit a polarity in receptor kinetic states in which ligand dissociation rates k_{off} at the pseudopod region are faster than at the tail region suggest that the SNR is higher at the pseudopod than at the tail [54].

The third and final way to improve SNR discussed in this section involves modulating the total amount of receptor expressed in cells (Fig. 2.7c). Increasing or decreasing the receptor number improves the SNR in the lower and higher concentration ranges of the chemoattractant, respectively. Receptor internalization too can contribute to SNR improvements in the higher concentration ranges. Also, receptor affinity for the chemoattractant is an important factor for adjusting the concentration ranges in chemotaxis (Fig. 2.7d). It is well known that cAMP receptors in *Dictyostelium* cells are phosphorylated upon cAMP stimulation, leading to a three- to approximately sixfold decrease in ligand-binding affinity [60]. Such an affinity shift of receptors contributes to an SNR increase in the higher-ligand-concentration range, which extends the response range to higher ligand concentrations. Thus, we can reveal the molecular mechanisms for both noise reduction and amplification in a stochastically operating signal transduction system by analyzing how the SNR is modulated depending on the kinetics properties of the signaling molecules.

2.6 Kinetic Heterogeneity of Signaling Molecules and Cellular Polarity

As described in Section 2.4, single-molecule imaging analysis of ligand-binding in cells has revealed multiple receptor kinetic states. For most G-protein-coupled receptors (GPCRs), the dissociation rates depend on the interaction of receptors with the coupled G-proteins [19, 22, 58], meaning ligand-binding kinetics can be used to elucidate the coupling of the receptors with G proteins. In membrane fractions that include the receptors and G proteins, ligand-binding kinetics is sensitive to the presence of GTP. In the absence of GTP, the receptors adopt

slow-dissociating states, where the receptors bind to G proteins but cannot facilitate their activation. The addition of GTP causes a shift in the receptor kinetic states from slow-dissociating to fast-dissociating states. This shift reflects the dissociation of G protein from the receptor via G protein activation. That is, the receptors adopt a slow-dissociating state with binding to G protein, while they adopt a fast-dissociating state when free from G protein. When G protein is efficiently activated, the receptor undergoes state transitions between the two.

For the case of cAMP receptors, ligand-binding kinetics using radiolabelled cAMP has identified at least two receptor kinetic states and that GTP addition to the membrane fractions increases fast-dissociating one [19]. We have performed single-molecule analysis of cAMP-binding kinetics on a membrane fraction to examine GTP sensitivity (Fig. 2.8a) [54]. In the absence of GTP, slow-dissociating states with dissociation rates of 0.4 s^{-1} or 0.08 s^{-1} were dominantly (78%) observed. GTP addition increased the fast-dissociating state with a dissociation rate of 1.3 s^{-1} up to 66%. When the membrane fractions prepared from the mutant cells lacking either functional G protein subunits $G\alpha_2$ or Gβ were used for this assay, GTP sensitivity was not observed, indicating that GTP-induced alterations in the cAMP-binding kinetics reflects altered interactions between the receptors and

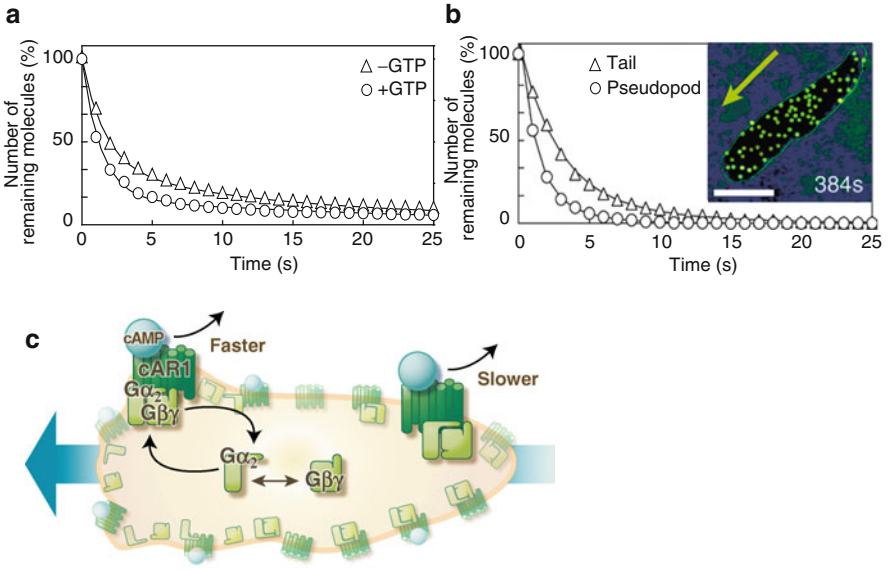

Fig. 2.8 Kinetic heterogeneity of cAMP bindings. (**a**) Cumulative probability distribution of Cy3-cAMP bound to the membrane fraction in the absence (*triangles*) and presence (*circles*) of GTP. (**b**) Cumulative probability distribution of Cy3-cAMP bound to the anterior pseudopod (*circles*) and posterior tail (*triangles*). (*inset*) Receptor occupancy in a chemotaxing cell. The positions of Cy3-cAMP bound to the receptor are shown by the *yellow dots*. (**c**) Schematic illustration of kinetic heterogeneity in Cy3-cAMP bindings. Faster and slower-dissociation of Cy3-cAMP in the anterior pseudopod and posterior tail, respectively, suggest high and low G protein activation.

their coupled G proteins. These results agree well with those obtained previously by conventional ligand-binding kinetics methods.

Based on these observations, we next examined the kinetic states of the receptor in chemotaxing cells by conducting single-molecule analysis of the cAMP-binding. Under a chemical gradient, *Dictyostelium* cells adopt a polarized shape with a pseudopod at the leading edge and a tail at the rear end (Fig. 2.8b). The cumulative probability distribution of Cy3-cAMP lifetimes was obtained separately for Cy3-cAMP molecules bound to the anterior and posterior halves of a polarized cell. As shown in Fig. 2.8b, the Cy3-cAMP lifetimes exhibited a polarity along the length of the cell. The lifetimes of Cy3-cAMP in the anterior region were about three times shorter than those in the posterior region. In the anterior region, the majority of the receptors adopted a fast-dissociating state with a dissociation rate of 1.1 s^{-1} (71%), while the remaining population of the receptor adopted a slow-dissociating state with a dissociation rate of 0.4 s^{-1} (29%). These dissociation rates resemble those observed in cAMP binding to membrane fractions in the presence of GTP, implying that receptors in the anterior region undergo cycling between G protein-bound and free states, and thus G proteins are efficiently activated at the anterior region. On the other hand, receptors in the posterior region adopted a slow-dissociating state with dissociation rates of 0.4 s^{-1} (76%) and 0.16 s^{-1} (24%), which resemble those observed in cAMP-binding kinetics on membrane fractions in the absence of GTP. This suggests that these receptors are somehow suppressed in their ability to activate G protein. Such polarity in the receptor kinetic states was not found in mutant cells lacking the $G\alpha_2$ or $G\beta$ subunits, suggesting that differences in the receptor states reflect on differences of the coupling with G-protein between the anterior and posterior regions. These results suggest anterior-posterior polarity affect the efficiency of G protein activation along with the length of a chemotaxing cell (Fig. 2.8c). Thus, single-molecule kinetic analysis can reveal the kinetic heterogeneity of signaling molecules within the context of a cell.

Anterior-posterior polarity in the receptor kinetic states may provide a molecular basis for noise-robust signal processing against the stochastic fluctuations seen in receptor occupancy. As described in Section 2.4, receptor occupancy in a cell undergoing chemotaxis towards a chemoattractant source is reversed spontaneously and transiently with respect to the direction of the gradient. If an anterior-posterior polarity affects the efficiency of G protein activation along the length of a cell, the ligand binding at the anterior pseudopod will preferentially affect cell behavior, while the transmembrane signaling at the posterior would be inefficient. Furthermore, polarity in receptor states may explain a polarity in the response to cAMP observed previously in the *Dictyostelium* cells [49]. Specifically, when a cell is stimulated locally with cAMP, it forms a pseudopod. At the anterior region of the cell, a pseudopod forms within a few seconds of cAMP stimulation, while if at the posterior region the formation takes about 40 s or more. This is consistent with the idea that transmembrane signaling by cAMP receptors is somehow inefficient at the posterior.

Such polar kinetic properties has been found in other signaling molecules such as the PtdIns(3, 4, 5)P_3-binding protein Crac and PTEN [27, 57]. Crac molecules stably localized at the pseudopod regions of a polarized cell undergoing chemotaxis

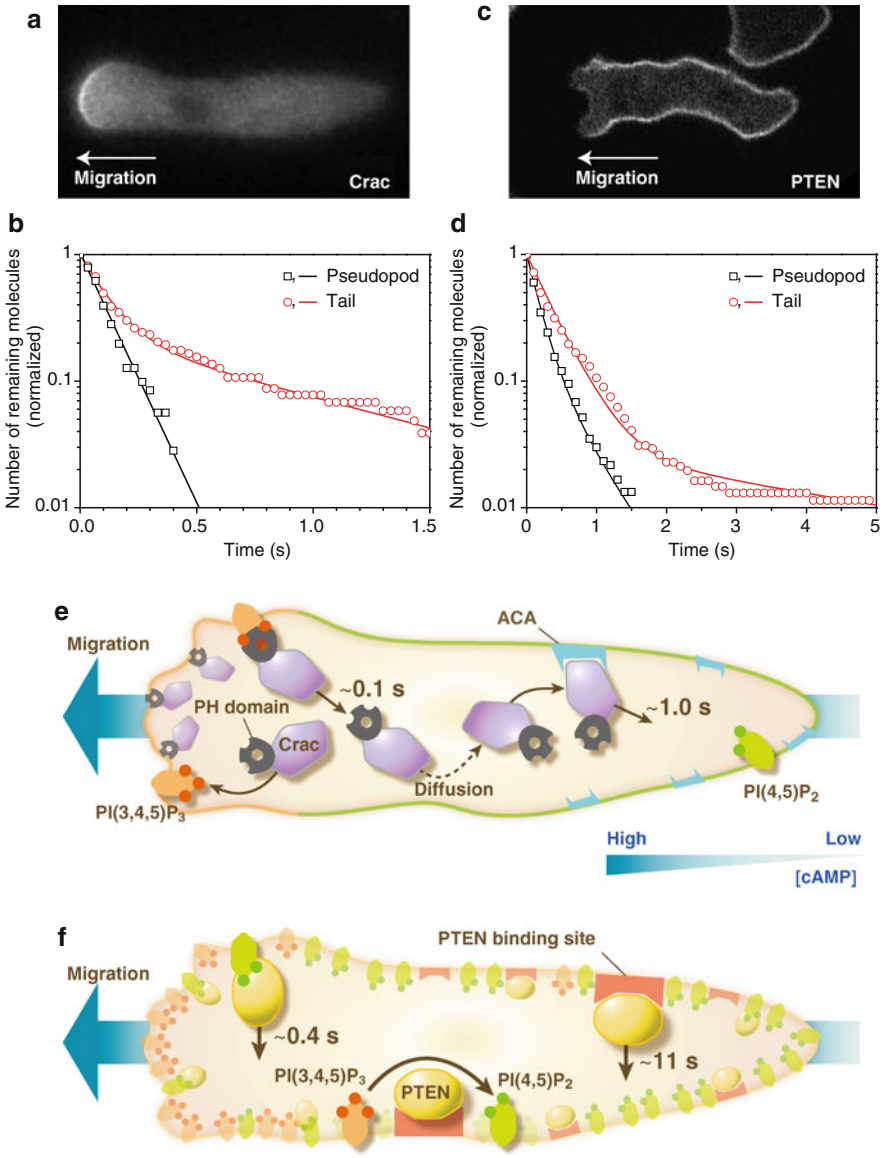

Fig. 2.9 Kinetic heterogeneities of downstream signaling molecules along the length of chemotaxing cells. (**a**) Localization of Crac-GFP at the anterior pseudopods of a polarized cell during chemotaxis. (**b**) Cumulative probability distributions of Crac-GFP in the anterior (*black squares*) and posterior halves (*gray circles*) of chemotaxing cells shown on a semi-logarithmic plot. (**c**) Localization of PTEN-TMR at the lateral and rear regions of a chemotaxing cell. (**d**) Cumulative probability distributions of PTEN-TMR in the anterior (*black squares*) and posterior halves (*gray circles*) of chemotaxing cells shown on a semi-logarithmic plot. (**e**) Schematic illustration of

when observed by conventional epi-fluorescence microscopy (Fig. 2.9a). The cumulative probability distribution of Crac, which was obtained by single-molecule observation, show that almost all Crac molecules dissociated from the anterior membrane within a lifetime of 110 ms (Fig. 2.9b). That is, stable localization of Crac at the pseudopod is maintained by rapid exchange of individual Crac molecules via dynamic shuttling between the membrane and cytosol. Crac molecules were also observed in the posterior regions by single-molecule imaging, which could not be seen when using conventional methods. The number of Crac molecules in the posterior region was ~30 times lower than that observed in the anterior region. The lifetimes of Crac molecules at the posterior regions were 110 ms (76%) and 890 ms (24%). Thus, fast-dissociation and slow-dissociation sites were preferentially localized at the leading edge and at the rear end of the polarized cells, respectively (Fig. 2.9e).

PTEN molecules also exhibit kinetic heterogeneity and dynamic shuttling between the membrane and cytosol. PTEN localized predominantly at the lateral and rear regions of a chemotaxing cell (Fig. 2.9c). Such stable localization is maintained by the shuttling of individual PTEN molecules. Lifetimes of PTEN molecules at the lateral and rear regions were 0.4 s (97%) and 11 s (3%), respectively, while the lifetime at the pseudopod regions was 0.2 ~0.6 s (Fig. 2.9d). Thus, even if the same signaling molecules are present at the anterior and posterior regions of a polarized cell, the signaling molecules adopt different kinetic states between the anterior and posterior regions (Fig. 2.9f).

The kinetic heterogeneity of downstream signaling molecules with relation to cellular polarity has the potential to modulate the quality of the transmitted signals and thus affect the corresponding molecular and cellular responses. As described in Section 2.5, downstream signaling reactions with faster kinetic rates can follow rapid temporal changes of upstream reactions, and thus cause effective noise propagation. On the other hand relatively slower reactions cannot follow such rapid temporal changes in the upstream reactions, leaving the noise from the upstream reactions to be averaged temporally. Thus, polarity in the kinetic heterogeneity of signaling molecules suggests that the anterior region may follow and respond to relatively faster and smaller changes in the environmental signals, while the posterior region may observe relatively slower and larger changes. That is, it is likely that the anterior region of chemotactic cells is more sensitive to environmental changes than the posterior one. The polarity in kinetic properties of signaling molecules downstream of the cascade may also provide a molecular basis for the robustness

Fig. 2.9 (continued) Crac membrane recruitment. Fast and slow-dissociation binding sites for Crac have been identified as PI(3,4,5)P_3 and adenylyl cyclase A (ACA) dependent, respectively. PI(3,4,5)P_3 and ACA-dependent sites are localized at the pseudopod and the tail of chemotaxing cells, respectively. (**f**) Schematic illustration of the kinetic heterogeneity of PTEN. PTEN molecules show fast-dissociation bindings, which depend on PIP_2, and slow-dissociation bindings, which are observed at the lateral and rear regions of chemotaxing cells.

against stochastic fluctuations seen in receptor occupancy and thus explain the polar responses made to chemotactic stimulations observed in *Dictyostelium* cells [49]. As a result, heterogeneity in the signaling molecules with relation to cellular polarity may further establish and maintain cellular polarity.

2.7 Conclusion Remarks

Here we take the chemotactic signaling of *Dictyostelium* cells as a typical example for stochastic signal processing and transduction in living cells. Single-molecule imaging analysis has revealed the kinetic properties of the signaling molecules responsible for chemotaxis. The GFR can be used to evaluate how these kinetic properties affect cellular chemotactic responses. Our analyses revealed that the stochastic properties of chemoattractant receptors most upstream of the chemotactic signaling cascade determine the chemotactic accuracy of the cells. The noise within transmembrane signaling by the receptors limits the precision of the directional sensing, suggesting that receptor-G protein coupling and its modulation have an important role on chemotaxis efficiency in cells. The noise generated at the ligand-receptor complex can be reduced through the slow dynamics of signaling molecules by using time-averaging effects. Overall, polarity within the kinetic heterogeneity of signaling molecules may provide a molecular basis for noise-robust signal processing.

Acknowledgments The authors thank all of the members of Stochastic Biocomputing Group in Osaka University for discussion and also thank Peter Karagiannis for critical reading of the manuscripts.

References

1. Axelrod D (2001) Total internal reflection fluorescence microscopy in cell biology. Traffic 2:764–774
2. Berg HC, Purcell EM (1977) Physics of chemoreception. Biophys J 20:193–219
3. Bialek W, Setayeshgar S (2005) Physical limits to biochemical signaling. Proc Natl Acad Sci USA 102:10040–10045
4. Devreotes PN, Zigmond SH (1988) Chemotaxis in eukaryotic cells: a focus on leukocytes and Dictyostelium. Annu Rev Cell Biol 4:649–686
5. Dormann D, Weijer CJ (2006) Imaging of cell migration. EMBO J 25:3480–3493
6. Eichinger L, Pachebat JA, Glockner G et al (2005) The genome of the social amoeba Dictyostelium discoideum. Nature 435:43–57
7. Fisher PR, Merkl R, Gerisch G (1989) Quantitative analysis of cell motility and chemotaxis in Dictyostelium discoideum by using an image processing system and a novel chemotaxis chamber providing stationary chemical gradients. J Cell Biol 108:973–984
8. Fornel F (2001) Evanescent waves. Springer, Berlin, Heidelberg, New York
9. Funatsu T, Harada Y, Tokunaga M et al (1995) Imaging of single fluorescent molecules and individual ATP turnovers by single myosin molecules in aqueous solution. Nature 374:555–559

10. Gerisch G (2009) Imaging actin cytoskeleton dynamics in Dictyostelium chemotaxis. Method Mol Biol 571:385–400
11. Graf R, Brusis N, Daunderer C et al (2000) Comparative structural, molecular, and functional aspects of the Dictyostelium discoideum centrosome. Curr Top Dev Biol 49:161–185
12. Hereld D, Jin T (2009) Chemotaxis. Methods Mol Biol 571. Humana Press, New York
13. Hibino K, Watanabe TM, Kozuka J et al (2003) Single- and multiple-molecule dynamics of the signaling from H-Ras to cRaf-1 visualized on the plasma membrane of living cells. Chemphyschem 4:748–753
14. Hibino K, Shibata T, Yanagida T et al (2009) A RasGTP-induced conformational change in C-RAF is essential for accurate molecular recognition. Biophys J 97:1277–1287
15. Howard PK, Ahern KG, Firtel RA (1988) Establishment of a transient expression system for Dictyostelium discoideum. Nucleic Acids Res 16:2613–2623
16. Iglesias PA, Devreotes PN (2008) Navigating through models of chemotaxis. Curr Opin Cell Biol 20:35–40
17. Iino R, Koyama I, Kusumi A (2001) Single molecule imaging of green fluorescent proteins in living cells: E-cadherin forms oligomers on the free cell surface. Biophys J 80:2667–2677
18. Janetopoulos C, Ma L, Devreotes PN et al (2004) Chemoattractant-induced phosphatidylinositol 3, 4, 5-trisphosphate accumulation is spatially amplified and adapts, independent of the actin cytoskeleton. Proc Natl Acad Sci USA 101:8951–8956
19. Janssens PM, Van Haastert PJ (1987) Molecular basis of transmembrane signal transduction in Dictyostelium discoideum. Microbiol Rev 51:396–418
20. Kitamura K, Tokunaga M, Iwane AH et al (1999) A single myosin head moves along an actin filament with regular steps of 5.3 nanometres. Nature 397:129–134
21. Kuwayama H, Yanagida T, Ueda M (2008) DNA oligonucleotide-assisted genetic manipulation increases transformation and homologous recombination efficiencies: Evidence from gene targeting of Dictyostelium discoideum. J Biotechnol 133:418–423
22. Levitzki A, Marbach I, Bar-Sinai A (1993) The signal transduction between beta-receptors and adenylyl cyclase. Life Sci 52:2093–2100
23. Lu HP, Xun L, Xie XS (1998) Single-molecule enzymatic dynamics. Science 282:1877–1882
24. Ma L, Janetopoulos C, Yang L et al (2004) Two complementary, local excitation, global inhibition mechanisms acting in parallel can explain the chemoattractant-induced regulation of PI(3, 4, 5)P3 response in dictyostelium cells. Biophys J 87:3764–3774
25. Manstein DJ, Titus MA, De Lozanne A et al (1989) Gene replacement in Dictyostelium: generation of myosin null mutants. EMBO J 8:923–932
26. Mato JM, Losada A, Nanjundiah V et al (1975) Signal input for a chemotactic response in the cellular slime mold Dictyostelium discoideum. Proc Natl Acad Sci USA 72:4991–4993
27. Matsuoka S, Iijima M, Watanabe TM et al (2006) Single-molecule analysis of chemoattractant-stimulated membrane recruitment of a PH-domain-containing protein. J Cell Sci 119:1071–1079
28. Matsuoka S, Miyanaga Y, Yanagida T et al (2008) Single-molecule imaging of stochastic events in living cells. In: Selvin PR, Ha T (eds) Single-molecule techniques. Cold Spring Harbor Laboratory Press, New York
29. Matsuoka S, Shibata T, Ueda M (2009) Statistical analysis of lateral diffusion and multistate kinetics in single-molecule imaging. Biophys J 97:1115–1124
30. McAnaney TB, Zeng W, Doe CF et al (2005) Protonation, photobleaching, and photoactivation of yellow fluorescent protein (YFP 10C): a unifying mechanism. Biochemistry 44:5510–5524
31. Miyanaga Y, Matsuoka S, Ueda M (2009) Single-molecule imaging techniques to visualize chemotactic signaling events on the membrane of living Dictyostelium cells. Method Mol Biol 571:417–435
32. Noegel AA, Schleicher M (2000) The actin cytoskeleton of Dictyostelium: a story told by mutants. J Cell Sci 113:759–766
33. Parent CA (2004) Making all the right moves: chemotaxis in neutrophils and Dictyostelium. Curr Opin Cell Biol 16:4–13
34. Parent CA, Devreotes PN (1999) A cell's sense of direction. Science 284:765–770

35. Postma M, Bosgraaf L, Loovers HM et al (2004) Chemotaxis: signalling modules join hands at front and tail. EMBO Rep 5:35–40
36. Rappel WJ, Levine H (2008a) Receptor noise limitations on chemotactic sensing. Proc Natl Acad Sci USA 105:19270–19275
37. Rappel WJ, Levine H (2008b) Receptor noise and directional sensing in eukaryotic chemotaxis. Phys Rev Lett 100:228101
38. Ridley AJ, Schwartz MA, Burridge K et al (2003) Cell migration: integrating signals from front to back. Science 302:1704–1709
39. Rosoff WJ, Urbach JS, Esrick MA et al (2004) A new chemotaxis assay shows the extreme sensitivity of axons to molecular gradients. Nat Neurosci 7:678–682
40. Sakmann B, Neher E (1995) Single channel recording. Plenum, New York
41. Sako Y, Yanagida T (2003) Single-molecule visualization in cell biology. Nat Rev Mol Cell Biol (Suppl):SS1–5
42. Sako Y, Minoghchi S, Yanagida T (2000) Single-molecule imaging of EGFR signalling on the surface of living cells. Nat Cell Biol 2:168–172
43. Sasaki AT, Firtel RA (2006) Regulation of chemotaxis by the orchestrated activation of Ras, PI3K, and TOR. Eur J Cell Biol 85:873–895
44. Sato MJ, Kuwayama H, van Egmond WN et al (2009) Switching direction in electric-signal-induced cell migration by cyclic guanosine monophosphate and phosphatidylinositol signaling. Proc Natl Acad Sci USA 106:6667–6672
45. Shaffer BM (1975) Secretion of cyclic AMP induced by cyclic AMP in the cellular slime mould Dictyostelium discoideum. Nature 255:549–552
46. Shibata T, Fujimoto K (2005) Noisy signal amplification in ultrasensitive signal transduction. Proc Natl Acad Sci USA 102:331–336
47. Song L, Nadkarni SM, Bodeker HU et al (2006) Dictyostelium discoideum chemotaxis: threshold for directed motion. Eur J Cell Biol 85:981–989
48. Swaney KF, Huang CH, Devreotes PN (2010) Eukaryotic chemotaxis: a network of signaling pathways controls motility, directional sensing, and polarity. Annu Rev Biophys 39:265–289
49. Swanson JA, Taylor DL (1982) Local and spatially coordinated movements in Dictyostelium discoideum amoebae during chemotaxis. Cell 28:225–232
50. Takagi H, Sato MJ, Yanagida T et al (2008) Functional analysis of spontaneous cell movement under different physiological conditions. PLoS One 3:e2648
51. Tokunaga M, Kitamura K, Saito K et al (1997) Single molecule imaging of fluorophores and enzymatic reactions achieved by objective-type total internal reflection fluorescence microscopy. Biochem Biophys Res Commun 235:47–53
52. Tranquillo RT, Lauffenburger DA, Zigmond SH (1988) A stochastic model for leukocyte random motility and chemotaxis based on receptor binding fluctuations. J Cell Biol 106:303–309
53. Ueda M, Shibata T (2007) Stochastic signal processing and transduction in chemotactic response of eukaryotic cells. Biophys J 93:11–20
54. Ueda M, Sako Y, Tanaka T et al (2001) Single-molecule analysis of chemotactic signaling in Dictyostelium cells. Science 294:864–867
55. Van Haastert PJ (1997) Transduction of the chemotactic cAMP signal across the plasma membrane. In: Maeda Y, Inouye K, Takeuchi I (eds) Dictyostelium. Universal Academy Press, Tokyo
56. Van Haastert PJ, Postma M (2007) Biased Random Walk by Stochastic Fluctuations of Chemoattractant-Receptor Interactions at the Lower Limit of Detection. Biophys J 93:1787–1796
57. Vazquez F, Matsuoka S, Sellers WR et al (2006) Tumor suppressor PTEN acts through dynamic interaction with the plasma membrane. Proc Natl Acad Sci USA 103:3633–3638
58. Waelbroeck I (1999) Kinetics versus equilibrium: the importance of GTP in GPCR activation. Trends Pharmacol Sci 20:477–481

59. Wazawa T, Ueda M (2005) Total internal reflection fluorescence microscopy in single molecule nanobioscience. Adv Biochem Eng Biotechnol 95:77–106
60. Xiao Z, Yao Y, Long Y et al (1999) Desensitization of G-protein-coupled receptors. agonist-induced phosphorylation of the chemoattractant receptor cAR1 lowers its intrinsic affinity for cAMP. J Biol Chem 274:1440–1448
61. Yanagida T, Ueda M, Murata T et al (2007) Brownian motion, fluctuation and life. Biosystems 88:228–242
62. Yumura S, Uyeda TQ (2003) Myosins and cell dynamics in cellular slime molds. Int Rev Cytol 224:173–225
63. Zigmond SH (1974) Mechanisms of sensing chemical gradients by polymorphonuclear leukocytes. Nature 249:450–452
64. Zigmond SH (1977) Ability of polymorphonuclear leukocytes to orient in gradients of chemotactic factors. J Cell Biol 75:606–616

http://www.springer.com/978-90-481-9863-4

Cell Signaling Reactions
Single-Molecular Kinetic Analysis
Sako, Y.; Ueda, M. (Eds.)
2011, X, 330 p., Hardcover
ISBN: 978-90-481-9863-4